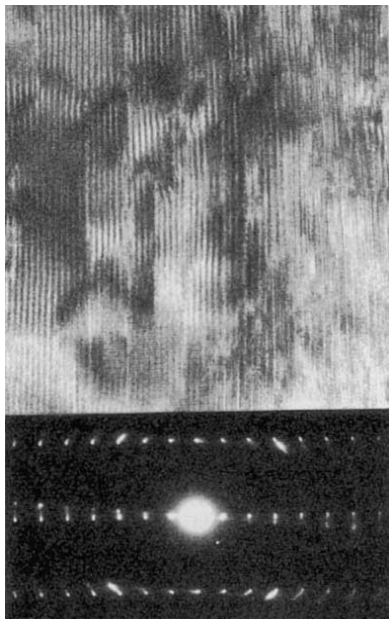

Fig. 3 Bright-field image orientated as in Fig. 2 of a $YBa_2Cu_3O_{7-x}$ specimen that has been exposed to the atmosphere for several days. Note the intense disorder and disruption of the parent structure. The corresponding orientated diffraction pattern (inset) shows streaking along c^* and rotation about the projection axis.

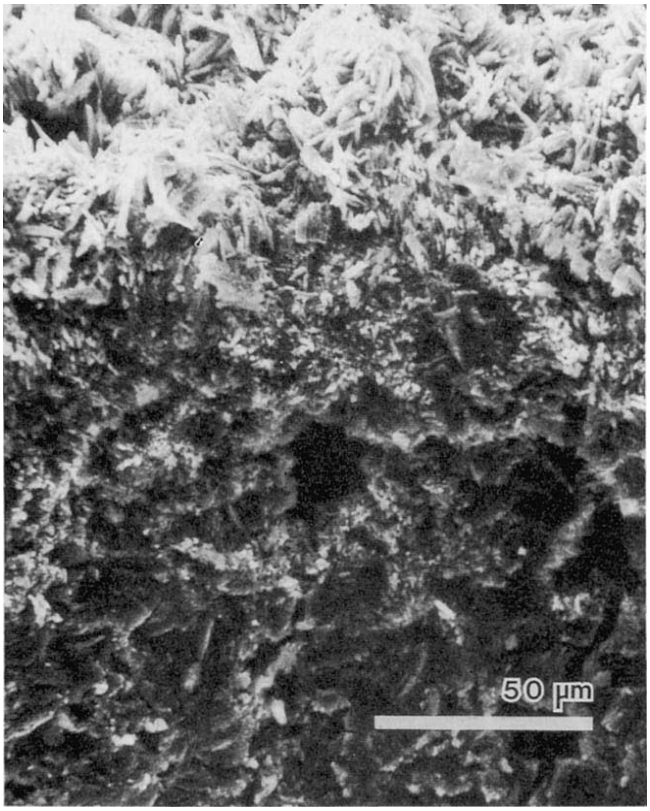

Fig. 4 Scanning electron micrograph (secondary electron image) at a fracture surface through a cold-pressed, sintered pellet of $YBa_2Cu_3O_{7-x}$ after accelerated atmospheric corrosion. The upper part of the micrograph exhibits the exposed surface of the pellet with micrometer-sized blade-like $BaCO_3$ crystals. The lower part shows the relatively uncorroded fracture surface with fissures and pores.

This result conflicts with the speculation[3] that the defects depicted there might be responsible for the superconductivity.

But we have also observed that the pure material deteriorates when exposed to the atmosphere, and that its degradation is manifested in two stages. In stage 1 defects appear in diffraction-contrast images, including planar faults parallel to (001) which, at higher magnifications, resemble some of those in the higher-resolution images in ref. 3. In our samples defect densities vary somewhat from grain to grain but, in general, fault density and depth of penetration into the crystals increase with further exposure. As shown in Fig. 3, this atmospherically degraded material gives rise to imperfect SADPs and lattice images. The streaking present along c^* in the SADP is matched in the lattice image by the planar defects parallel to (001), while the rotation about the projection axis corresponds to the waviness of the lattice fringes 'perpendicular' to c^*.

Stage 2 is the bulk decomposition of the 90-K superconducting phase. Products of its decomposition in air have been identified by X-ray powder diffraction as $Ba_2Cu(OH)_6$, $BaCO_3$, CuO and $Y(OH)_3$. Studies of enhanced degradation in air at 40 °C saturated with water vapour have shown that bulk decomposition begins at the surface, from which microcrystals of $BaCO_3$ grow. Figure 4 shows a scanning electron microscope image of the surface of the degraded specimen.

Our measurements and qualitative observations demonstrate that the presence of defects is not a pre-requisite for 'high-temperature' superconductivity in this new class of superconducting materials, and suggest that at least some of the observed defects are characteristic of the decomposition of the superconducting phase, rather than of the pure material itself.

Superconductivity may still be observed, even in the partly degraded material, as long as continuous electrical pathways exist. But the exclusion of water vapour is clearly of prime importance in any consideration of potential applications of this high-temperature superconductor.

We acknowledge the technical assistance of Mr Peter Barlow, Mr Roger Heady for the SEM micrograph, and of Miss Caroline Twang.

Received 4 May; accepted 19 May 1987.

1. Dickman, S., Swinbanks, D., Lindley, D. & Pease, R. *Nature* **326**, 432-433 (1987).
2. Strongin, M., Welch, D. O. & Emergy, V. J. *Nature* **326**, 540-541 (1987).
3. Ourmazd, A. *et al. Nature* **327**, 308-310 (1987).

High electrical conductivity in doped polyacetylene

N. Basescu*, Z.-X. Liu*, D. Moses,* A. J. Heeger*, H. Naarmann† & N. Theophilou†

Department of Physics and *Institute for Polymers and Organic Solids, University of California, Santa Barbara, Santa Barbara, California 93106, USA
†BASF Laboratories, Ludwigshafen, FRG

The electrical conductivity of conducting polymers results from mobile charge carriers introduced into the π-electron system through doping[1,2]. Because of the large intra-chain transfer integrals, the transport of charge is believed to be principally along the conjugated chains, with inter-chain hopping as a necessary secondary step. In conducting polymers, as in all metals and semiconductors, charge transport is limited by a combination of intrinsic electron–photon scattering and sample imperfection. Although relatively high conductivities ($\sigma \approx 1{,}000\ S\ cm^{-1}$) have been reported for partially orientated and heavily doped polyacetylene[1–3], the absence of a metal-like temperature dependence implies that the observed values are not intrinsic. In doped polyacetylene,

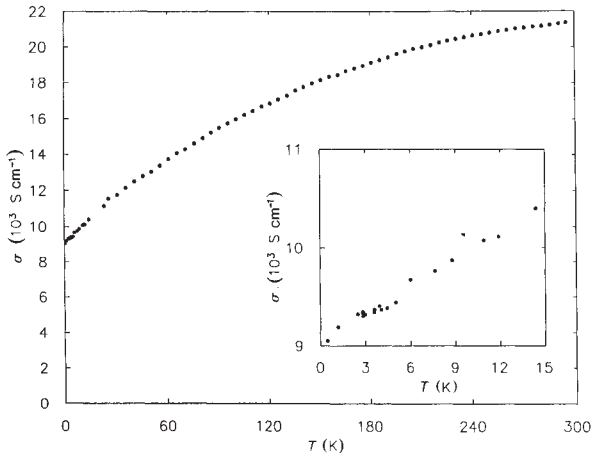

Fig. 1 $\sigma_{\parallel}(T)$ for a fourfold stretched sample at 10 kbar; the inset shows the temperature dependence below 4 K in more detail. At room temperature, the conductivity is greater than 20,000 S cm^{-1}; at 0.5 K the conductivity is still above 9,000 S cm^{-1}.

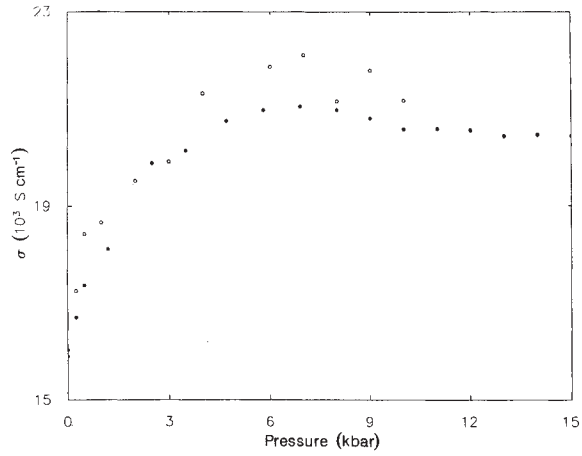

Fig. 2 Pressure dependence of $\sigma_{\parallel}$ at room temperature from 1 atm to 15 kbar. Solid dots and open circles represent two independent samples with stretching ratios of 6:1.

$(CH)_x$, electrical transport can be limited both by microscopic defects (leading to scattering and localization) and by the more macroscopic complex fibrillar morphology[12] and associated interfibrillar contacts. Thus, with improvements in material quality, one might anticipate corresponding improvements in the electrical conductivity. Here we report the synthesis of polyacetylene with fewer sp^3 defects than in material prepared by other methods. The higher-quality material exhibits substantially higher electrical conductivity; maximum values of >20,000 S cm^{-1} are obtained after doping with iodine. The conductivity has been measured as a function of temperature and pressure: at 0.48 K and 10 kbar, iodine-doped samples remain highly conducting ($\sigma \approx$ 9,000 S cm^{-1}).

Free-standing polyacetylene films (thickness ~30 μm) were synthesized using the Zeigler–Natta catalyst technique, initially developed by Shirakawa and colleagues[4], with important modifications introduced by Naarmann[5]. The catalyst (tetrabutoxytitanium, 31 ml, and triethylaluminium, 41 ml, suspended in silicone oil, 50 ml) was stirred for two hours at 120 °C, followed by stirring and degassing (pumping) while cooling slowly to room temperature. The polymerization reaction was carried out at room temperature (rather than using[4] toluene with polymerization at −78 °C) in a controlled atmosphere drybox, followed by washing to remove all the catalyst (3 hours in toluene followed by 16 hours in methanol containing 6% HCl, and finally two periods of 1–1.5 hours each with methanol. The resulting films are roughly a 50/50 mixture of *cis*- and *trans*-polyacetylene; elemental analysis: C, 91.7–92.2%; H, 7.6–7.7%; O, <0.5%; Al/Ti, 0.01%. Isomerization to the all-*trans* material can be achieved by subsequent heating or by doping. The material can be stretch-oriented with maximum elongation ratio of about 6:1.

The polymer synthesized by this technique has been thoroughly characterized[5]. In most respects it is essentially identical to polyacetylene prepared by the Shirakawa technique. The material has the characteristic fibrillar morphology (approximately the same fibril diameter as Shirakawa material) with a density of 0.5 g cm^{-3}. X-ray scattering studies show features which are indistinguishable from Shirakawa material. The principal difference is a major reduction in the number of sp^3 defects to a level which is not detectable by high-resolution ^{13}C nuclear magnetic resonance. No bands corresponding to —CH_3— or —CH_2— could be detected at wavelengths of 2,960, 2,910 and 2,830 μm in the infrared spectrum. The low density of sp^3 defects implies a higher degree of chain perfection in this material.

The $(CH)_x$ films were doped to saturation by immersion for one hour in a saturated solution of iodine in CCl_4, followed by rinsing three times in pure solvent for two minutes each. Since $(CCl_3)^-$ is produced in the photon catalysed reaction, $2I_2 + CCl_4 \rightarrow (CCl_3)^- + ICl$, and attacks the double bonds on the polyacetylene chain, care must be taken not to expose the solution to light. Weight uptake analysis indicates a doping concentration of $y \approx 0.06$ assuming a composition of $[(CH)^{+y}(I_3^-)_y]_x$; we find that most of the doping occurs during the first 15 minutes of immersion. Immersion in the iodine solution for more than 70–80 minutes yields films with lower conductivity, possibly due to degradation of the polymer.

Immediately after rinsing, four copper wires were attached to the doped film (under an inert atmosphere) using electrodag. The samples, mounted with the stretch direction either parallel ($\sigma_{\parallel}$) or perpendicular ($\sigma_{\perp}$) to the current flow, were placed in a teflon cell for high pressure measurements (1 atm to 15 kbar). The pressure cell was designed for interchangeable use in a closed cycle Displex refrigerator for measurements from 20K to 300K and in a ^{3}He cryostat for measurements down to 0.48K.

The most striking feature of the Naarmann polyacetylene is the high electrical conductivity. Figure 1 shows $\sigma_{\parallel}$ as a function of temperature for a fourfold stretched sample at 10 kbar. At room temperature, the conductivity is greater than 20,000 S cm^{-1}; at 0.5 K the conductivity is still above 9,000 S cm^{-1}. The inset shows the temperature dependence below 4K in more detail. The results shown in Fig. 1 are typical, with good reproducibility from sample to sample. For a single sample, the conductivity was observed to decrease monotoni-

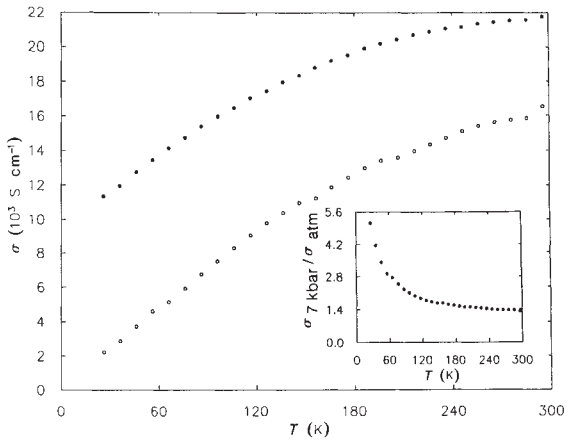

Fig. 3 Temperature dependence of $\sigma_{\parallel}$ at 7 kbar (solid dots) and at 1 atm (open circles); stretching ratio 6:1. Pressure suppresses the decrease in $\sigma_{\parallel}(T)$ at low temperatures. Inset: $[\sigma_{\parallel}(7\text{ kbar})/\sigma_{\parallel}(1\text{ atm})]$ as a function of temperature.

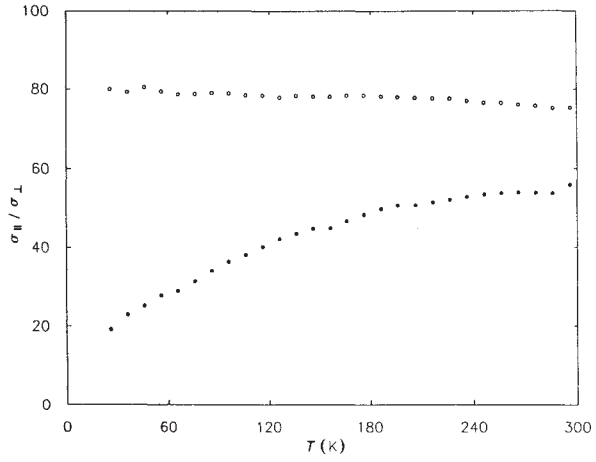

Fig. 4 Temperature dependence of $(\sigma_\parallel/\sigma_\perp)$ for pressures of 1 atm (solid dots) and 7 kbar (open circles); stretching ratio 6:1.

cally with time (down by about 30% over a period of a week) indicative of the irreversible degradation known for iodine doping[1,2].

Figure 2 shows the pressure dependence of $\sigma_\parallel$ at room temperature from 1 atm to 10 kbar. The parallel conductivity has a gentle maximum at about 7 kbar; the data are reversible on cycling up to 15 kbar. The perpendicular conductivity (not shown) increases by about 10% below 1 kbar and remains constant (within measurement error) at higher pressures. The pressure dependence of $\sigma_\parallel$ and $\sigma_\perp$ was checked on a number of different samples and found to be characteristic.

Figure 3 shows the temperature dependence of $\sigma_\parallel$ at several different pressures; high pressure suppresses the decrease in $\sigma_\perp(T)$ at low temperatures. This effect is emphasized in the inset to Fig. 3 where we plot the ratio $[\sigma_\parallel(7\text{ kbar})/\sigma_\parallel(1\text{ atm})]$ as a function of temperature.

The anisotropy of the conductivity is relatively large compared to that obtained from previous measurements on material prepared by the Shirakawa method; we find $(\sigma_\parallel/\sigma_\perp) \approx 80$ at 7 kbar. The anisotropy is somewhat higher at high pressure, as $\sigma_\parallel$ increases with pressure while $\sigma_\perp$ remains essentially constant. The temperature dependence of $(\sigma_\parallel/\sigma_\perp)$ is shown in Fig. 4 for pressures of 1 atm and 7 kbar. Note that at high pressure, the ratio is constant.

The observation of a temperature- and pressure-dependent anisotropy suggests that the transport data are beginning to provide information on intrinsic processes. The magnitude and temperature independence of $\sigma_\parallel(T)$ below 1 K implies genuine metallic behaviour for heavily doped polyacetylene (consistent with specific heat[6], thermopower[7] and susceptibility data[8]) and rules out transport by hopping among strongly localized states. Note, however, that $\sigma_\parallel(T)$ increases with increasing temperature implying that phonon-assisted transport (either through microscopic localized states or across inter-fibrillar barriers) is involved. Thus, although this modified synthesis yields significantly higher-quality polyacetylene (with $\sigma_\parallel$ within about a factor of 20 of the conductivity of copper) the transport is still limited by material imperfection.

Although improvement of solid-state properties through higher-quality materials is a general feature of materials science, there has been little optimism that this rule would be applicable to conducting polymers. Perhaps the reason for this was the argument that the high level of impurities in doped conducting polymers would negate any improvements towards molecular chain perfection. The present study demonstrates that this is not the case in polyacetylene or (by implication) in other conducting polymers: the achievement of still higher-quality material from improved synthesis and processing can be expected to lead to correspondingly better electronic properties.

The research at UCSB was supported by the Office of Naval Research.

Note added in proof: H.N. recently announced further improvements in the preparation of oriented polyacetylene leading to a room temperature electrical conductivity of $\sim 1.5 \times 10^{+5}$ S cm^{-1} with an anisotropy of $\sim 10^3$ (*American Chemical Society Meeting Symposium on Conducting Polymers, Their Emergence and Future*; April 7-8, 1987, Denver, Colorado).

Received 3 February; accepted 23 March 1987.

1. Skotheim, T. J. (ed.) *Handbook of Conducting Polymers* (ed. Skotheim, T. J.) (Dekker, New York, 1986).
2. Etemad, S., Heeger, A. J. & MacDiarmid, A. G. *A. Rev. Phys. Chem.* **33**, 443 (1982).
3. Gould, C. M. *et al. Phys. Rev.* B **23**, 6820 (1981).
4. Shirakawa, H. & Ikeda, S. *Synth. Met.* **1**, 175 (1980).
5. Naarmann, H. *Synth. Met.* **17**, 223 (1987).
6. Moses, D., Denenstein, A., Pron, A., Heeger, A. J. & MacDiarmid, A. G. *Solid St. Commun.* **36**, 219 (1980).
7. Park, Y. W., Denenstein, A., Chiang, C. K., Heeger, A. J. & MacDiarmid, A. G. *Solid St. Commun.* **29**, 747 (1979).
8. Moraes, F., Chen, J., Chung, T.-C. & Heeger, A. J. *Synth. Met.* **11**, 271 (1985).

Lightning triggered from the Earth's magnetosphere as the source of synchronized whistlers

W. C. Armstrong

STARLAB, 324 Durand Building, Stanford University, Stanford, California 94305, USA

Specific patterns established by natural radio signals echoing periodically in a magnetospheric whistler duct[1-3] are sometimes observed to indicate strongly preferred times at which identical, well-defined whistlers occur. Ordinarily such whistlers would be assumed to originate in the stronger ground strokes[4] of spontaneous lightning. These nonrandom whistlers are therefore unexpected and raise the possibility that some whistler-source discharges may be triggered from the magnetosphere. The same possibility could also be predicted independently from another type of our recent observations. Selected examples of nonrandom whistlers are given here and the supporting observations described. In the absence of a previously developed theoretical explanation, a trigger mechanism is outlined which emphasizes discontinuous discharge to the upper atmosphere[5]. Such a mechanism might help explain several related phenomena.

Examples to be shown are from Southern Hemisphere data recorded at Siple Station, Antarctica, 76° S, 84° W geographic. Two nearly identical whistlers W_1 and W_2 occur in Fig. 1, each arriving about two seconds after its Northern Hemisphere source discharge. The second (W_2) is approximately in phase with echoes due to the first (W_1). If many whistlers were found with phasing identical to W_2, then their source discharges could no longer be thought of as spontaneous. Here, solid diagonal lines repeat a base period measured near 3.0 kHz between the leading edges of W_1 and its 'two-hop echo', e_1.

Because they are quickly eroded by path-propagation losses, successive echoes e_1-e_5 weaken and collapse toward a single frequency. This illustrates two important points: first, if periodic signals are to continue echoing in a long train, supplemental energy usually is required and second, if a unique period is maintained, it is usually because of a dominant signal echoing at a single frequency. Here 'echo' E_2 shows supplemental energy mostly at constant frequency. The starting time of E_2 shows that the leading edge of W_1 has established the periodicity.

With energy now being added, each echo grows gradually and becomes more complex until E_5 (not labelled) and supplemental emission T_2 result. W_2 appears to follow precisely in phase with T_2, so a Northern Hemisphere source discharge might be triggered in connection with T_2's northern reflection.